(22) Hjertberg, T.; Sandberg, M.; Wennerstrom, O.; Lagerstedt, I. *Synth. Met.* **1987**, *21*, 31.
(23) Baughman, R. H.; Wolf, J. F.; Eckhardt, H.; Shacklette, L. W. *Synth. Met.* **1988**, *25*, 121.
(24) Tan, K. L.; Tan, B. T. G.; Kang, E. T.; Neoh, K. G. *Phys. Rev. B* **198**., *39*, 8070.
(25) Kang, E. T.; Neoh, K. G.; Khor, S. H.; Tan, K. L.; Tan, B. T. G. *J. Chem. Soc., Chem. Commun.* **1989**, 696.
(26) Neoh, K. G.; Kang, E. T.; Khor, S. H.; Tan, K. L. *Polym. Degrad. Stab.* **1990**, *27*, 107.
(27) Kang, E. T.; Ti, H. C.; Neoh, K. G. *Polym. J.* **1988**, *20*, 845.
(28) Ng, K. T.; Hercules, D. M. *J. Am. Chem. Soc.* **1975**, *97*, 4168.
(29) Matsunaga, Y. J. *J. Chem. Phys.* **1964**, *41*, 6.
(30) Foster, R. *Organic Charge Transfer Complexes*; Academic Press: New York, 1969; 313 and references therein.
(31) Street, G. B.; Clark, T. C.; Krounbi, M.; Kanazawa, K. K.; Lee, V.; Pfluger, P.; Scott, J. C.; Weiser, G. *Mol. Cryst. Liq. Cryst.* **1982**, *83*, 253.
(32) Kang, E. T.; Neoh, K. G.; Tan, T. C.; Ong, Y. K. *J. Polym. Sci., Polym. Chem. Ed.* **1987**, *25*, 2143.
(33) Foster, R. *Organic Charge Transfer Complexes*; Academic Press: New York, 1969; Chapter 4.

Registry No. O_2, 7782-44-7; HCl, 7647-01-0; polyaniline (homopolymer), 25233-30-1; polyaniline (SRU), 32036-19-4; chlorine, 7782-50-5; *o*-chloranil, 2435-53-2; *o*-bromanil, 2435-54-3.

On the Mechanism of Craze Fibril Breakdown in Glassy Polymers

Larry L. Berger

E. I. du Pont de Nemours and Company, Inc., Central Research and Development Department, Experimental Station, Wilmington, Delaware 19898

Received August 3, 1989; Revised Manuscript Received December 15, 1989

ABSTRACT: Optical and transmission electron microscopy were used to investigate the mechanism of craze fibril growth and breakdown in a series of neat glassy polymers of poly(methyl methacrylate) (PMMA), poly(α-methylstyrene) (PαMS), and polystyrene (PS), as well as in fully compatible blends of poly(2,6-dimethyl-1,4-phenylene oxide) (PPO) and PS, all at a homologous $T_g - T = 75$ °C. The neat polymers were examined over a broad range of molecular weight M, and the PPO–PS system was studied as a function of the weight fraction of PPO (ϕ) in the blend. During a slow strain rate test, in which ~40 independent film squares were simultaneously monitored, the median tensile strains at which crazing, ϵ_c, and craze fibril breakdown, ϵ_b, occurred in each polymer were determined. For the neat polymers, with $M < M_c$ (where M_c is the critical molecular weight for entanglement effects on the zero-shear rate viscosity) no stable craze formation was observed (i.e., $\epsilon_b - \epsilon_c \approx 0$); for $M \approx (2\text{–}20)M_c$, $\epsilon_b - \epsilon_c$ increased strongly with M and at $M > 20M_c$, $\epsilon_b - \epsilon_c$ increased only weakly with increasing M. For the PPO–PS blends, ϵ_c was found to be roughly constant for $0.5 < \phi < 0.68$ whereas $\epsilon_b - \epsilon_c$ increased markedly at values of $\phi \geq 0.64$. In all cases, craze fibril breakdown was traced to the formation of a small pear-shaped void at the craze/bulk interface. The morphology and statistics of the craze breakdowns were combined with a detailed description of the craze microstructural parameters (i.e., the craze fibril diameter and craze fibril spacing) to advance a molecular model of craze breakdown. At these strain rates, craze breakdown is believed to occur by two events: (1) random chain scission to form the surfaces of the craze fibrils and (2) stress-mediated chain disentanglement, of a group of surviving strands, *at the craze/bulk interface*. The predictions of this model are in satisfactory agreement with the empirically determined molecular weight (or ϕ) dependence of ($\epsilon_b - \epsilon_c$).

Introduction

It is now well established that brittle fracture in many glassy polymers can be traced to the formation and subsequent breakdown of small fibrillated regions of stress-induced plastic deformation, crazes.[1-9] Consequently, the importance of crazing in controlling the macroscopic postyield mechanical properties of polymers remains an area of keen interest.[10] In particular, recent studies examining the role of molecular entanglements and the polymer network on craze growth have shed new light on the mechanism of craze fibril formation and the factors that govern the scale of fibrillation.[10-15] In contrast, however, our understanding of craze fibril breakdown is quite poor.

Generally it has been recognized that the process of craze growth gives rise to two unique regions within the craze:[1-4,9,16-18] (1) the craze/bulk interfaces, a thin (ca. 10–25-nm) strain-softened polymer layer in which craze fibrillation (and hence craze widening) takes place and (2) the craze midrib, a thin (ca. 50–100-nm-wide) polymer layer lying in the center of the craze, which forms immediately behind the advancing craze tip. It should be emphasized that an important distinction exists between these two regions. Namely, the relative position of the craze midrib does not change as the craze widens. On the other hand, as the craze boundaries advance by drawing fresh polymer from this interface, it continuously generates a new locally strain-softened region, concomitantly leaving behind the now strain-hardened craze fibrils. Thus, unlike the craze midrib, the immediate location of the craze boundaries is a function of the plastic strain. While these two regions can be readily distinguished by microscopic techniques, there is poor agreement as to the site of the early stages of craze breakdown.

Previous studies involving calculations of the stress field at the crack tip,[19-21] optical interferometry measurements of the advance of the craze tip in precracked samples,[22-24] morphological examinations of fracture surfaces,[2,16,18,25] and acoustic emission analysis have proposed,[26] from indirect measurements or theory, a microscopic mechanism of craze fibril breakdown. Recently,

0024-9297/90/2223-2926$02.50/0

however, a comprehensive study[5,6] of craze breakdown in thin films of polystyrene (PS) offered some of the first direct measurements of craze fibril stability and breakdown. In that study, Yang et al. examined the detailed process of craze breakdown in thin films of PS with nearly monodisperse molecular weight distributions and in binary blends of high and low molecular weight PS. An important result of that study was the unambiguous determination that the site of craze breakdown invariably lies at the craze/bulk interface and not in the craze midrib. This result differed from that of theoretical studies on PS[21] and experimental studies on poly(methyl methacrylate) (PMMA),[22-24] the latter of which involved interferometric measurements of crack growth in precracked samples. In those studies craze breakdown was attributed to a fibril creep or slippage process along the craze midrib.

Yang et al.,[5,6] in addition to examining the morphology of craze breakdown in PS, used optical microscopy to simultaneously monitor the craze fibril stability in a large number of independent film squares. Hence, statistical information on craze breakdown could be obtained. Moreover, using low-angle electron diffraction (LAED) techniques, they carefully characterized the microstructure and periodicity of the crazes produced in these samples. In turn, the empirically determined scale of fibrillation within the craze was used to determine the mean number of effectively entangled strands, n_e, per unit cross section along the fibril, that *survived* fibrillation. At the slow rates used in those experiments it was argued that the initial chain scission which is required to produce the surfaces of the craze fibrils was not sufficient to produce the observed craze fibril breakdown. Instead it was hypothesized that craze breakdown occurred by random chain scission of entangled strands followed by chain disentanglement of the surviving strands at the craze boundary. On the basis of these ideas and the microscopic measurements of craze fibril stability, Yang et al.[5,6] proposed a molecular model of craze fibril breakdown. A key result of this model was the prediction that the craze fibril stability, for both the monodisperse PSs and the binary blends of PS, could be uniquely correlated with n_e; a result in apparent agreement with the data. Unfortunately, however, the claim was based on an incorrect determination of n_e (in the blends). A replot of the data reveals that while the craze fibril stability increases strongly with n_e, this single parameter does not provide a good correlation for the two sets of data.[10] Nevertheless, their approach, particularly the role of chain disentanglement at the craze/bulk interface, provided new insight on the molecular process of craze breakdown.

In this paper, we use a technique similar to that developed by Yang et al.[5,6] to investigate the craze fibril stability and the early stages of craze fibril breakdown in a series of nearly monodisperse films of PMMA, PαMS, and PS, as well as in fully compatible blends of poly(2,6-dimethyl-1,4-phenylene oxide) (PPO) and PS. For each of these samples, the craze microstructure and the craze fibril dimensions have been independently characterized.[15] Here we present the salient modifications and expansion of the recently revised statistical microscopic model[10] of Yang et al.[5,6] and discuss the generality of this approach for other glassy thermoplastics.

Experimental Section

The following polymer glasses, having a glass transition temperature T_g and entanglement density ν_e ($=\rho N_a/M_e$, where ρ is the density of the polymer, N_a is Avogadro's number, and M_e is the entanglement molecular weight $\approx {}^1/_2 M_c$), as displayed in Table I, were used in this study:

Table I[a]

polymer	T_g, °C	$10^{-25}\nu_e$, strands/m^3
PαMS	175	4.8*
PMMA	110	7.8
PS	100	3.3
PPO–PS (M_w = 4K)		
ϕ	135	3.7**
ϕ = 0.6	147	5.3
ϕ = 0.64	152	6.1
ϕ = 0.68	157	6.8

[a] Determined from M_e values given in refs 38 (*) and 8 (**).

1. A series of nearly monodisperse poly(methyl methacrylates) (PMMAs) were purchased from the Pressure Chemical Co. (*) and Scientific Polymer Products Inc. (**), having a weight-average molecular weight M_w (and molecular weight distribution M_w/M_n) = 27.3K (1.1)*, 63.9K (1.08)*, 107K (1.1)*, 330K (1.11)**, 480K (1.09)*, 700K (1.09)**, 2600K (~1.9), and 5200K (1.3). The two highest molecular weight samples were specially prepared in a laboratory synthesis and subsequently characterized by gel permeation chromatography and light-scattering methods.

2. A series of nearly monodisperse poly(α-methylstyrenes) (PαMSs) were purchased from the Pressure Chemical Co. (*), Scientific Polymer Products Inc. (**), and Polymer Laboratories (***), having a weight average molecular weight M_w (and M_w/M_n) = 23K (1.1)*, 76.5K (1.1)*, 133K (1.05)**, 425K (1.1)*, 641K (1.1)*, 1250K (1.1)***, and 1420K (1.18)*.

3. A series of nearly monodisperse polystyrenes (PSs) were purchased form the Pressure Chemical Co., having a weight average molecular weight M_w (and M_w/M_n) = 90K (1.1), 400K (1.06), and 1860K (1.12).

4. Compatible blends of a poly(2,6-dimethyl-1,4-phenylene oxide) (PPO) have a M_n = 32K and of a PS have a M_w = 4K (M_w/M_n = 1.06); the PPO was obtained from Scientific Polymer Products, Inc., and the PS, from the Pressure Chemical Co. Blends consisting of PPO with weight fraction ϕ = 0.5, 0.6, 0.64, and 0.68 were examined. (At values of $\phi > 0.7$, the samples deformed by shear deformation and not crazing.)

Dilute solutions of each molecular weight of PMMA, PαMS, and PS in methylene chloride and blends of PPO–PS in chloroform were prepared and successively filtered through a 5- and 0.75-μm-pore-size filter. Thin films of all of the above polymers were prepared by drawing rigorously cleaned glass slides from the appropriate solutions at a constant rate. In all cases, a film thickness of ~0.6 μm was produced by adjusting the viscosity of the solutions. The films were floated off onto the surface of a filtered water bath and picked up on well-annealed copper grids, the bars of which were previously coated with the same polymer. After drying, a brief exposure of the films to the vapor of the solvent served to provide good adhesion between the grid bars and the film. Subsequently, all of the samples were physically aged at 90 °C, under vacuum, for 15 h prior to straining.

For the measurements of the craze fibril stability, grids consisting of at least 40 film squares, which were free of either dust particles or other perceptible imperfections, were used. These samples were enclosed in a controlled-temperature environment and deformed at a constant strain rate of 4.0×10^{-6} s^{-1} and $T_g - T$ = 75 °C. About hourly observations were made, in situ, using a reflected light microscope at 50× magnification to determine the cumulative number fraction of grid squares that exhibited crazing, P_c, and craze fibril breakdown, P_b.[5,6] At this magnification the onset of crazing and craze growth could be readily detected. Typically, however, the smallest regions of craze fibril breakdown that could be routinely observed were roughly 10–20 μm in diameter. While these observations do not correspond to the earliest stages of craze breakdown, as will be discussed later, transmission electron microscopy (TEM) studies of samples strained up to P_b = 0.5 demonstrate that this optical criterion is generally a reliable indicator of the first event of craze breakdown within a film square.

Subsequent to straining, individual film squares were isolated and examined with transmission electron microscopy (TEM)

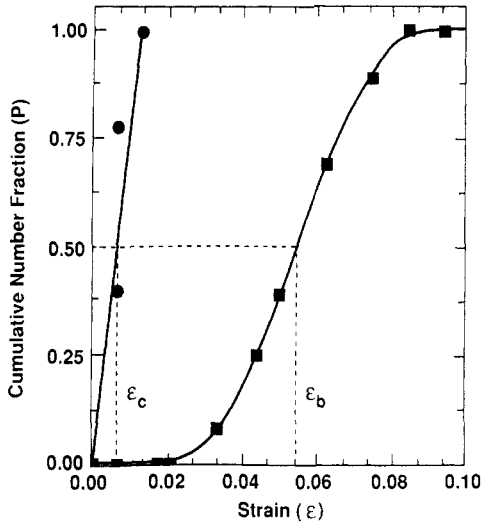

Figure 1. Plot of the cumulative number fraction of grid squares exhibiting crazing, P_c (●), and craze fibril breakdown, P_b (■), as a function of strain, ϵ, for a PMMA sample with a molecular weight M of 480K deformed at a rate of 4.0×10^{-6} s^{-1} and $T_g - T = 75$ °C.

using a JEOL 2000EX fitted with a LaB_6 filament and operated at 200 kV. In all cases the lowest possible illumination conditions were used. For PMMA, which is a positive electron resist, even under these conditions only a limited TEM survey was possible.

Results

Statistics of Craze Breakdown. A plot of the cumulative number fraction of grid squares exhibiting crazing P_c (filled circles) and craze fibril breakdown P_b (filled squares) as a function of strain ϵ for a PMMA sample with a molecular weight M of 480K deformed at $T_g - T = 75$ °C and a rate of 4.0×10^{-6} s^{-1} are shown in Figure 1. These data correspond to a single sample consisting of ~40 independent film squares. As illustrated, the value of P_c was observed to increase linearly with strain reaching a value of unity at $\epsilon_p = 0.02$. By comparison, the curve corresponding to craze breakdown P_b typically exhibited a sigmoidal curvature with increasing ϵ. Also indicated in this plot are the values of the median tensile strain for craze formation, ϵ_c, and craze fibril breakdown, ϵ_b, corresponding to $P_c = 0.5$ and $P_b = 0.5$, respectively. As will be shown later, the full distribution of P_b vs ϵ contains valuable information about the increase in the drawing stress of the film with increasing plastic strain.

A plot of the critical strain to produce crazing, ϵ_c (filled circles), and the craze fibril stability, $\epsilon_b - \epsilon_c$ (filled squares), versus log M for the PMMA samples, deformed at a rate of 4.0×10^{-6} s^{-1}, is shown in Figure 2. It can be seen that for $M \geq M_c$ (where M_c is the critical molecular weight for entanglement effects on the zero-shear rate viscosity) ϵ_c was observed to remain roughly constant at about 0.01. On the other hand, the strain to produce craze fibril breakdown ($\epsilon_b - \epsilon_c$) was observed to exhibit a pronounced molecular weight dependence. For $M < M_c$, no stable craze formation was observed (i.e., $\epsilon_b - \epsilon_c \approx 0$); at intermediate molecular weights $\epsilon_b - \epsilon_c$ increased strongly with increasing M, from $\epsilon_b - \epsilon_c = 0.015$ at $M = 27$K to $\epsilon_b - \epsilon_c = 0.05$ at $M = 107$K, and at a higher molecular weights, i.e., $M > 20M_c$, $\epsilon_b - \epsilon_c$ increased only weakly with increasing M.

Shown in Figures 3 and 4 are plots of ϵ_c (filled circles) and $\epsilon_b - \epsilon_c$ (filled squares) versus log M for the series of PαMS and PS samples, with narrow molecular weight distributions, respectively. Here also the samples were

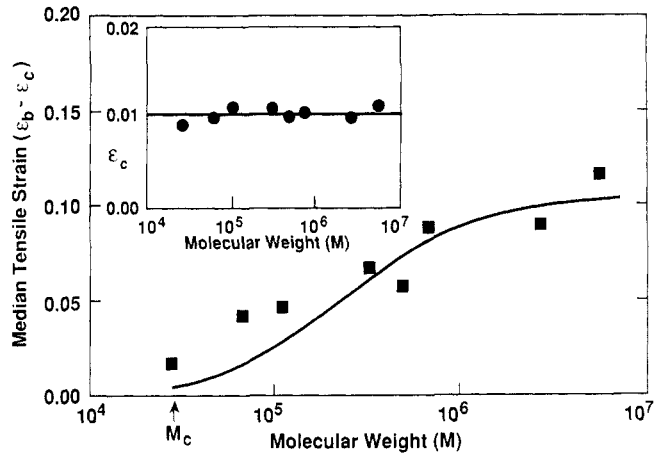

Figure 2. Plot of median tensile strain for crazing, ϵ_c (●), and craze fibril breakdown, $\epsilon_b - \epsilon_c$ (■), versus log (molecular weight) for the PMMA samples deformed at a rate of 4.0×10^{-6} s^{-1} and $T_g - T = 75$ °C.

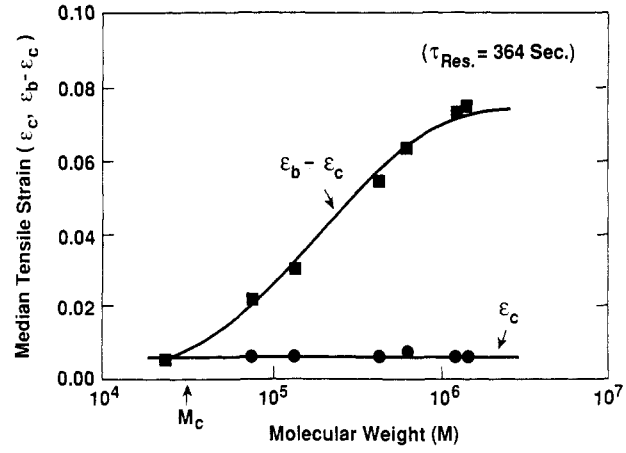

Figure 3. Plot of median tensile strain for crazing, ϵ_c (●), and craze fibril breakdown, $\epsilon_b - \epsilon_c$ (■), versus log (molecular weight) for the PαMS samples deformed at a rate of 4.0×10^{-6} s^{-1} and $T_g - T = 75$ °C. The solid curve drawn through the $\epsilon_b - \epsilon_c$ data was computed using eq 10 and a value of $\tau_{res} = 364$ s.

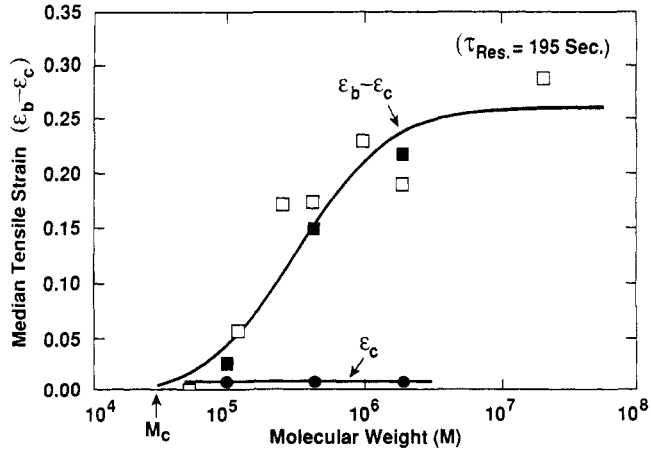

Figure 4. Plot of median tensile strain for crazing, ϵ_c (●), and craze fibril breakdown, $\epsilon_b - \epsilon_c$ (■), versus log (molecular weight) for the PS samples deformed at a rate of 4.0×10^{-6} s^{-1} at $T_g - T = 75$ °C. Also shown are the values of $\epsilon_b - \epsilon_c$ (□) from Yang et al. given in ref 5. The solid curve drawn through the $\epsilon_b - \epsilon_c$ data was computed using eq 10 and a value of $\tau_{res} = 195$ s.

deformed at $T_g = T = 75$ °C and at a rate of 4.0×10^{-6} s^{-1}. As can be seen, the behavior observed in these polymers was qualitatively similar to that observed in PMMA. That is, for $M > M_c$, ϵ_c exhibited no apparent molecular

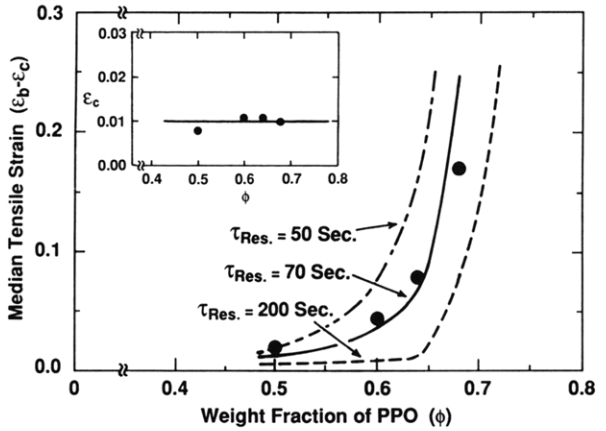

Figure 5. Plot of median tensile strain for crazing, ϵ_c (●), and craze fibril breakdown, $\epsilon_b - \epsilon_c$ (■), versus weight fraction of PPO (ϕ) in the PPO–PS blends deformed at a rate of 4.0×10^{-6} s^{-1} and $T_g - T = 75$ °C. Curves drawn through the $\epsilon_b - \epsilon_c$ data were computed using eq 10 and a τ_{res} value of 50 (– · –), 70 (—), and 200 s (- - -).

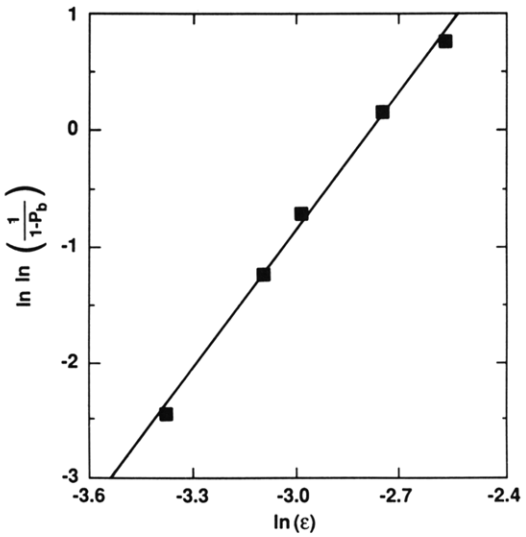

Figure 6. Weibull plot, ln (ln $(1/(1 - p_b))$) versus ln ϵ_p, of the data shown in Figure 1. The Weibull modulus, ρ_w, and Weibull scale parameter, ϵ_w, are determined from the slope and y intercept, respectively.

weight dependence whereas $\epsilon_b - \epsilon_c$ was observed to increase strongly at intermediate M and only weakly at higher M. Also included in Figure 4 are some previous data, of Yang et al. (□),[5] on PS samples deformed at a comparable temperature and strain rate. As can be seen, there is good agreement between the two sets of data.

A plot of the median tensile strains to produce crazing ϵ_c (filled circles) and craze fibril breakdown $\epsilon_b - \epsilon_c$ (filled squares) for the PPO–PS blends, deformed at $T_g - T = 75$ °C and at a rate of 4.0×10^{-6} s^{-1}, is shown in Figure 5. Here the value of ϵ_c was roughly constant at 0.01 for weight fractions of PPO (ϕ) between 0.5 and 0.68. (At lower values of ϕ only brittle films were produced, whereas at higher values of ϕ the films deform by shear and not crazing.) By comparison the craze fibril stability ($\epsilon_b - \epsilon_c$) exhibited a marked dependence on ϕ; specifically at $\phi = 0.6$, $\epsilon_b - \epsilon_c = 0.04$, whereas at $\phi = 0.68$ $\epsilon_b - \epsilon_c$ increased to 0.17.

A Weibull plot, ln (ln $(1/(1 - P_b))$) versus ln ϵ_p, of the data shown in Figure 1 for $0 < P_b < 1.0$ is displayed in Figure 6. From a least-squares fit to this curve, two parameters, the Weibull modulus, ρ_w, and the Weibull scale parameter, ϵ_w, may be extracted from the slope and y intercept, respectively. It has previously been shown[5,6] that the values of ρ_w and ϵ_w are measures of the breadth of the distribution of craze breakdown and the craze strength, respectively. For PMMA a value of $\rho_w = 3.5$ was determined; moreover, this value was found to be independent of M. On the other hand, the value of ϵ_w (not shown) was found to increase with increasing M, essentially mirroring that of ϵ_b. Similar Weibull plots were constructed for the PαMS, PS, and PPO–PS blends from which values of ρ_w, equal to 4.4, 4.0, and 3.8, respectively, were determined. Here too the values of ρ_w were found to be independent of M, in agreement with previous work, whereas the values of ϵ_w mirrored that of ϵ_b.[5,6]

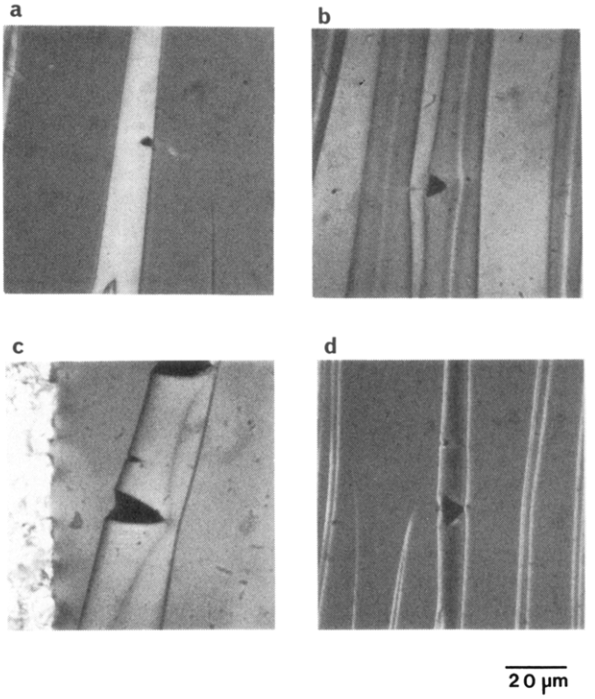

Figure 7. Optical micrographs of examples of craze fibril breakdown in PMMA (a), PαMS (b), PS (c), and a PPO-PS blend with $\phi = 0.68$ (d). In each case craze breakdown can be traced to a small pear-shaped void at the craze bulk interface.

Optical and Transmission Electron Microscopy Observations of Craze Breakdown. The early stages of craze fibril breakdown were examined using transmission electron microscopy TEM and high-magnification (i.e., 1000×) optical microscopy. In particular for PMMA, which is a positive electron resist, the latter technique was preferred.

For these observations, the samples were strained up to $P_b = 0.5$, and suitable individual grid squares were selected and examined. At the slow strain rates used in these experiments wide crazes, typically 10–30 μm in width, could be grown. Almost invariably, the craze fibril breakdowns could be traced to the formation of a small pear-shaped void at the craze/bulk interface and not in the craze midrib. The morphology of the "pear" is such that the widest portion is oriented toward the advancing interface. Typical examples of craze breakdown in films of PMMA, PαMS, PS, and PPO–PS (with $\phi = 0.68$) are shown by the optical micrographs in Figure 7a–d. When viewed in reflected light, the small voids appear as dark cavities. (Because the voids can cause the plane of the film to be directed away from the objective lens of the optical microscope, the cavities often appear larger than the actual void, thus facilitating their detection.) Examples of earlier stages of craze breakdown in PαMS, PS, and a PPO–PS sample with $\phi = 0.68$ are shown by the

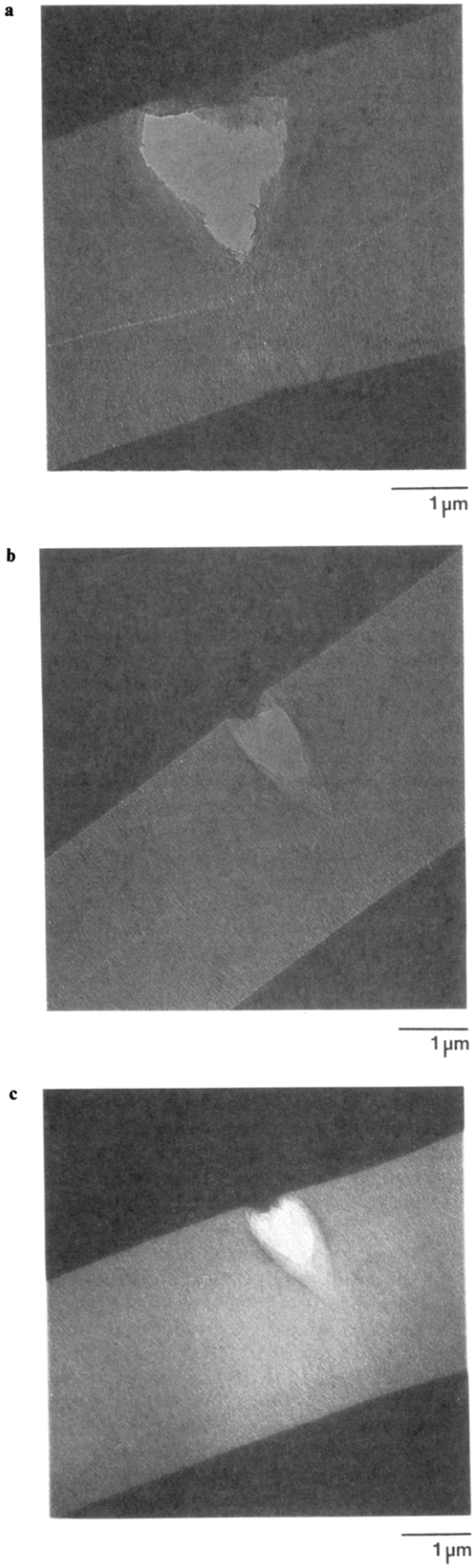

Figure 8. Transmission electron micrographs of craze fibril breakdown in PαMS (a), PS (b), and a PPO–PS blend with ϕ = 0.68 (c). Note, the site of the craze breakdowns is at the craze/bulk interface.

TEM micrographs in Figure 8a–c. At the values of ϕ examined here, all of the PPO–PS samples exhibited a qualitatively similar craze breakdown morphology.

A closer examination of the craze breakdown sites revealed that in most cases these breakdowns appeared to nucleate at an intrinsic flaw within the polymer glass and were not associated with a foreign (dust) inclusion. However, despite the special care that was taken in these experiments to eliminate foreign particles in the film, in a small number of cases, the craze breakdowns were associated with these inclusions. Generally, these craze breakdowns were of two types: For the larger inclusions (>1–2 μm), voids were typically observed to form at the craze/bulk interface invariably at the point at which the inclusion interrupted the polymer fibrillation. In rare cases, however, small dust particles (<0.5 μm) were found to be incorporated into the craze; subsequently, at higher strains, these particles were observed to debond from the film. Consequently a small cavity would be produced away from the craze/bulk interface. Nevertheless, here too, the voids were not traced to the craze midrib.

Discussion

It is well established that craze widening in air occurs by drawing fresh polymer from the craze/bulk interface at a nearly constant extension ratio.[3–11] At temperatures well below T_g, the advance of this interface and the concomitant formation of the craze fibril surfaces accompanies a significant loss of entangled strands from the polymer network.[3,4,7,11] This loss occurs in the locally strain-softened boundary where isotropic polymer is transformed into small highly oriented craze fibrils. Recent studies have shown that both the scale of fibrillation within the craze and the magnitude of the crazing stress, as well as the effects of temperature, strain rate, and strand density, are adequately described by a variant of the Taylor meniscus instability mechanism.[3,4,10,28–30] This process of craze widening (fibrillation) continues, uninterrupted, until the craze boundary encounters a flaw in the glass, which is sufficient to produce a craze breakdown.

As discussed above, both TEM and optical microscopy reveal that the site of the craze fibril breakdowns, in PαMS, PMMA, and PS and in the PPO–PS blends, invariably lies at the craze/bulk interface. These morphological observations of craze breakdown, i.e., at the craze/bulk interface, are in qualitative accord with recent experimental work on craze breakdown in PS;[5,6] however, it differs from that of other studies on PS[21] and PMMA.[21–24] In the latter cases, based on either theoretical predictions or indirect measurements, craze breakdown was attributed to a fibril creep or slippage process at the craze midrib. Clearly, that mechanism of craze breakdown was not observed in our film squares. Moreover, the pear-shaped morphology of the craze breakdown site observed here is consistent with fractograhic studies of crack formation, at slow strain rates, in unprecracked bulk samples of PMMA[18] and PS.[2,16,18]

From the morphological evidence of craze breakdown at the craze/bulk interface it seems clear that an important variable governing craze fibril stability is the mean number of effectively entangled strands, n_e, that survive the formation of the fibril surfaces. Following Yang et al.,[5,6] we[10] calculate n_e by first considering the total number of effectively entangled strands within the (starting) undeformed phantom fibril element, n_o, viz.

$$n_o = {}^1/_8 \pi d \nu_e (D_o)^2 \quad (1)$$

where d is the rms end-to-end distance of an entangled strand with mass M_e (the entanglement molecular weight),

Table II[a]

polymer	d, nm	D_o, nm	q
PαMS	8.6	21.5*	0.643**
PMMA	7.3	17.7	0.632
PS	9.6	19.0	0.598
PPO–PS (M_w = 4K)			
ϕ = 0.5	8.4	22.1	0.661
ϕ = 0.6	8.0	24.5	0.706
ϕ = 0.64	7.3	25.8	0.738
ϕ = 0.68	7.0	26.7	0.752

[a] From refs 15 (*) and 31 (**).

ν_e is the entanglement density ($=\rho N_a/M_e$, where ρ is the density of the polymer and N_a is Avogadro's number), and D_o is the average craze fibril spacing, which has been previously determined for these polymers.[15] For PMMA, PαMS, PS, and the blends of PPO–PS the values of d and D_o are listed in Table II. Using eq 1, the calculated values of n_o are found to be in the range of 25–125.

In turn, the number of entangled strands that survive fibrillation, n_e, can be computed from the following expression:[10]

$$n_e = n_o q(1 - M_e/(qM_n)) \tag{2}$$

where q, previously given by Kuo et al.[31] as a function of D_o/d, is the fraction of the n_o strands that survive fibrillation and M_n is the number average molecular weight of the starting polymer. This form of n_e is consistent with the expectation that the number average molecular weight of polymer chains in the craze fibrils, M_n', following the random chain scission at the craze boundary, is given by

$$1/M_n' = 1/M_n + (1 - q)/M_e \tag{3}$$

For the polymers examined here the values of q, listed in Table II, are typically in the range of 0.5–0.75. (Consequently, for a PMMA or PS sample with a molecular weight of 1000K, M_n' is on the order of 30K.)[32]

A simple estimate of the probability $P_s(0)$ that all of the strands within a given fibril (transfer length) fail by chain scission can be computed from the following:[3,10]

$$P_s(0) = (1 - q)^{n_e/q} \tag{4}$$

Now if one uses the values of n_e and q, for the crazes formed in either PS, PαMS, or PMMA or in the PPO–PS blends to compute $P_s(0)$ and in turn $\epsilon_b - \epsilon_c$, the values obtained are on the order of 6–10 orders of magnitude too large. Hence, the initial chain scission that occurs in forming the craze fibril surfaces is not sufficient to produce the observed craze fibril breakdown.

Logically, two other possibilities exist for generating the additional strand loss which is required to produce a craze fibril breakdown: namely, further thermally activated chain scission or chain disentanglement processes *in the active zone*. As argued by Yang et al.,[5,6] the former seems unlikely since for the strands that survive fibrillation the average force per entangled strand is well below the bond strength ($\approx 6 \times 10^{-9}$ N) along the polymer backbone. Moreover, any additional chain scission would be expected to occur with equal likelihood throughout the length of the fibril and not be localized at the craze boundary. However, as discussed above, craze breakdown was invariably traced to the craze/bulk boundary.

On the other hand, recent high-temperature crazing experiments[11–14] have inarguably demonstrated that polymer chain mobility at the craze/bulk boundary (the so-called active zone) is possible, although difficult to measure directly. In those experiments it was observed that at sufficiently slow strain rates and at temperatures near but below T_g a transition from scission-dominated to disentanglement-dominated crazing occurred; moreover, the disentanglement was shown to be localized in the active zone. It was argued that the presence of the voided surface at the boundary may be expected to relax the topological constraints on the polymer chains and in turn decrease the monomeric friction coefficient, ζ_o, of the chains in this region. Here too, we reasonably expect that the fluidlike value of ζ_o for the chains within the active zone will be reduced and subsequently will rise to a higher value as the fibril is drawn and strain hardened. (In fact, given the typical values of fibril dimensions and n_e (ca. 35–70), polymer chains are on the order of at most only a few nearest neighbors from a free surface.) The idea that polymer chain mobility at the craze boundary may be sufficient to generate the additional strand loss, which is required to produce craze failure, is consistent with the expectation of an enhanced mobility.

Recognizing that the onset of craze fibril breakdown results from a loss of integrity of the entanglement network within the fibrils, we now consider the probability P_{SD} that a craze fibril fails when a bundle of i strands survive fibrillation and subsequently these i strands disentangle, viz.[10]

$$P_{SD} = \sum_{i=0}^{i=n_e/q} P_{survival}(i)\, P_{dis}(i) \tag{5}$$

where $P_{survival}$ is the probability that i strands survive and P_{dis} is the probability that they subsequently disentangle. The term P_{dis} can be approximated by the expression[10]

$$P_{dis}(i) \approx \exp(-t_{dis}/\tau_{res}) \tag{6}$$

where τ_{res} is an effective residence time at the craze boundary. Physically τ_{res} can be thought of as the time in which the fluidlike value of ζ_o rises to a much higher value approaching that which is characteristic of the strain hardened glass. From appropriate scaling arguments it has recently be shown that, for the high stresses that are present at the craze boundary during fibrillation, a reasonable form for $t_{dis}(i)$ is[10,33,34]

$$t_{dis}(i) = \frac{\zeta_o l_o}{24}\left(\frac{M(i)}{M_o}\right)^2 \frac{i}{F}\left\{3 + \ln\left(1 + \frac{M(i)}{2M_e}\right)\right\} \tag{7}$$

where F is the force on the fibril ($=^1/_4 S_c \pi (D_o)^2$, S_c is the crazing stress), l_o is the monomer length, and $M(i)$ is the number average molecular weight of the group of i strands.[36] It can be seen that for high molecular weights t_{dis}, which reflects a stress-mediated disentanglement process, scales as M^2.[33]

It is reasonable to expect that $P_{survival}$ will be given by a discrete binomial distribution which, in turn, we approximate using a continuous normal distribution, viz.[10]

$$P_{survival}(i) = \frac{1}{[2\pi n_e(1 - q)]^{1/2}} \exp\left\{\frac{-(i - n_e)^2}{2(1 - q)n_e}\right\} \tag{8}$$

Now if we define the continuous reduced variable $\beta \equiv i/n_e$, eq 5 can be rewritten as[10]

$$P_{SD} = n_e \int_0^{1/q} P_{survival}(\beta)\, P_{dis}(\beta)\, d\beta \tag{9}$$

where P_{dis} and $P_{survival}$ are given by eqs 6 and 8, respectively.

As shown in the Appendix, one can relate the empirically determined Weibull parameters to the statistical

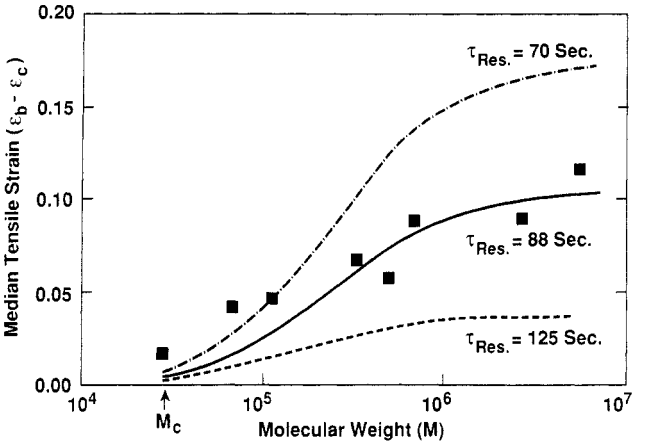

Figure 9. Plot of median tensile strain for craze fibril breakdown, $\epsilon_b - \epsilon_c$ (■), versus log (molecular weight) for the PMMA samples. Curves drawn through the data were computed using eq 10 and a τ_{res} value of 70 (- · -), 88 (—), and 125 s (- - -).

description of craze breakdown given above and derive the following expression for the craze fibril stability ($\epsilon_b - \epsilon_c$), viz.[10]

$$\epsilon_b - \epsilon_c = \left[\frac{\rho_w(\lambda - 1)\ln 2}{P_{SD}(S_1)n_f V_0}\right]^{1/\rho_w} \tag{10}$$

where $P_{SD}(S_1)$ is the probability that a fibril fails when a group of i strands break and subsequently disentangle at a drawing stress S_1 (corresponding to a plastic strain $\epsilon_p = 1$), λ is the craze fibril extension ratio,[8-10] ρ_w is the Weibull modulus, V_0 is the initial volume of the film square ($\approx 6 \times 10^{-13}$ m^3), and n_f [$\approx (dD_o^2)^{-1}$] is the number of fibril transfer lengths per unit risk volume V.

All of the parameters in eqs 9 and 10, except P_{dis} particularly through the quantity [$\zeta/F\tau_{res}$] in eq 6, are known or can be directly computed. We proceed by estimating S_c and thus F ($=^1/_4 S_c \pi (D_o)^2$) from[11]

$$S_c \approx 8\Gamma/D_0 \tag{11}$$

where Γ is the total craze surface ($=\gamma_S + d\nu_e U_b/4$, γ_S is the van der Waals surface energy, and U_b is the bond energy along the polymer backbone).[3] Next, from previous studies of the disentanglement-dominated high-temperature crazing behavior in PS,[10,11] we estimate the value of ζ_o at $T_g - T = 75$ °C; subsequently this value will be used for the other polymers. At this point the only unknown that remains in eq 10 is τ_{res}, which we will adjust to produce the best fit to the data. It should be emphasized that uncertainties in the absolute values of F and ζ_o will simply shift the value of τ_{res} needed to fit the data but will otherwise not affect the functional dependence of P_{SD}.

An example of this fitting procedure for the plot of the craze fibril stability ($\epsilon_b - \epsilon_c$) versus molecular weight for PMMA is shown in Figure 9. Three curves of $\epsilon_b - \epsilon_c$, computed using eq 10 and values of τ_{res} = 70, 88, and 125 s, are drawn through the data. As can be seen, a value of τ_{res} = 88 s produced the best fit. Generally it was observed that the magnitude of τ_{res} only shifted the predicted $\epsilon_b - \epsilon_c$, up or down, but did not significantly alter the shape of the curve, in agreement with the experimental data. Additional insight into the functional dependence of eq 10 can be gained by examining the molecular weight dependence of the P_{SD}. Shown in Figure 10 is a plot of the computed P_{SD} for the three values of τ_{res} that were used in generating the curves drawn in Figure 2. It can be seen that in all cases the P_{SD} drops rapidly (several orders of magnitude) over the same molecular

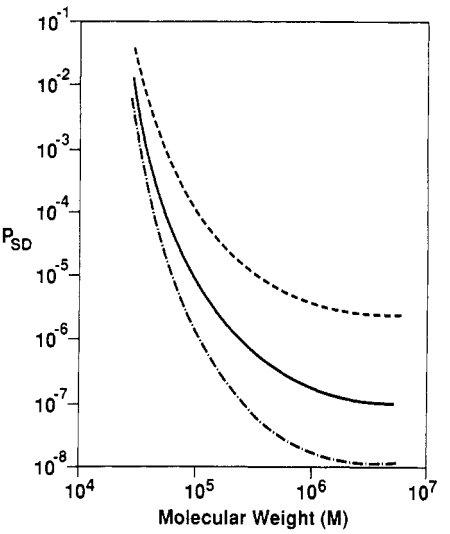

Figure 10. Plot of the molecular weight dependence of P_{SD} for the PMMA samples; the curves shown were computed using eq 9 and a value of τ_{res} = 70 (- - -), 88 (—), and 125 s (- · -).

weight range in which the craze fibril stability increases and ultimately levels off (i.e., at $\sim M > 20M_c$). Furthermore, at the lowest molecular weights, where the P_{SD} is relatively large, the fit obtained using eq 10 is only modestly dependent on τ_{res}. Hence, the computed curves of $\epsilon_b - \epsilon_c$ are only weakly dependent on τ_{res} at low molecular weights.

Using eq 10, similar fits to the molecular weight dependence of $\epsilon_b - \epsilon_c$ for PαMS and PS are shown by the solid curves in Figures 3 and 4, respectively. For these polymers the values of τ_{res} that produced the best fit were 364 s for PαMS and 195 s for PS. Here again it can be seen that the computed curves successfully predict the strong increase in craze fibril stability at intermediate M and the weak dependence at the highest values of M. In view of the physical constraints on the single adjustable parameter τ_{res}, the agreement between the model and the empirical data over the wide molecular range is quite satisfactory.

Additionally, eq 10 may be used to predict the craze fibril stability ($\epsilon_b - \epsilon_c$) in the blends of PPO and PS. Shown in Figure 5, as a solid line, is the computed curve of $\epsilon_b - \epsilon_c$ versus the weight fraction of PPO in the blend (ϕ) that was obtained using a value of τ_{res} = 70 s, which produced the best fit.[37] Two additional curves corresponding to τ_{res} values of 50 and 200 s are also shown. Here again it can be seen that where the P_{SD} is large, i.e., at low values of ϕ, the computed craze fibril stabilities are only modestly dependent on τ_{res}. Nonetheless, the predicted dependence of $\epsilon_b - \epsilon_c$ on ϕ, particularly the sharp increase in $\epsilon_b - \epsilon_c$ for values of $\phi > 0.64$, is in reasonable agreement with the experimental results.

The advantage of this model[10] vis-à-vis that which was originally proposed by Yang et al.[5,6] is 2-fold: Namely, their implicit assumption that P_{dis} was independent of the number of i strands that survive the initial chain scission is physically unreasonable. In that approach, the probability that a given entangled strand survived fibrillation was simply computed as the product of the *independent* probabilities that the strand survived scission and subsequently survived disentanglement. In fact, that result led them to the unique correlation of $\epsilon_b - \epsilon_c$ with n_e for both the monodisperse PSs and the binary blends of PS; a result that is not borne out by the data (when the correct values of n_e in the blend are used). The more complete description outlined above explicitly takes into

account the force per (remaining) strand and its corresponding stress-mediated disentanglement time, as well as the starting molecular weight of the polymer chains.[38]

While the proposed model is in satisfactory agreement with the empirical measurements of the craze fibril stability, clearly additional experimental and theoretical studies are needed to explore the crucial role of polymer chain mobility in the active zone as well as during the strain hardening of the small (ca. 6–15-nm-diameter) craze fibrils. Although recent experiments[11-14] have convincingly demonstrated that the inherently large surface to volume ratio of chains in the craze fibrils will lead to properties different from that of the bulk, our knowledge in this area remains quite sketchy. For example, the qualitative trend of the τ_{res} values needed to fit the craze fibril stability data, i.e., $(\tau_{res})_{PS} > (\tau_{res})_{PMMA} \sim (\tau_{res})_{PPO}$, would suggest that the effective monomeric friction coefficients of PMMA and PPO would be higher than in PS. While this trend is qualitatively consistent with diffusion[39] and rheological[40] data for the same polymers at a homologous $T_g - T$, before a quantitative comparison can be made further studies are needed to explore the mechanistic differences between chain dientanglement under the high stresses at the craze interface and that in the melt.

Additionally, it should be noted that several simplifying assumptions were made in deriving eqs 6–10. Namely, it was assumed that each bond breakage along the polymer backbone produced two free radicals, which subsequently neither cross-link with neighboring chains nor depolymerize by unzipping. Cross-linking could have the effect of producing branching or otherwise increasing the molecular weight of the chains in the fibrils whereas unzipping may be expected to have the opposite effect. Thus, the validity of this assumption for bond breakage in PS, as well as in polymers having an α-methyl group substituent (e.g., PαMS and PMMA), where unzipping can occur, requires additional study.

Last, in developing eq 10, the role of crosstie fibrils, i.e., the fibrils that link nearest-neighbor main fibrils, was not considered. However, it is known that the crosstie fibrils constitute roughly 10–15% of the craze volume.[41,42] Neglecting these fibrils will produce an overestimate of the amount of strand loss that occurs during fibrillation and, more importantly, will not allow for the transferring of the load between bridging fibrils. The former effect will decrease the value of q in eqs 2 and 3 (by ~10–15%) and thus may be expected to have only a small effect; however, the latter effect is more difficult to assess quantitatively. Certainly, a more detailed molecular model of craze fibril breakdown will need to consider the role of the crosstie fibrils.

Conclusions

The morphology and statistics of craze fibril breakdown were determined in thin films of neat PMMA, PαMS, and PS as well as in fully compatible blends of PPO–PS, all at a homologous $T_g - T = 75$ °C. The neat polymers were examined over a broad range of molecular weight M, and the PPO–PS system was studied as a function of the weight fraction of PPO (ϕ) in the blend. For the neat polymers with $M < M_c$, no stable craze formation was observed; for $M \approx (2\text{–}20)M_c$, the craze fibril stability ($\epsilon_b - \epsilon_c$) increased strongly with M, and for $M > 20M_c$, $\epsilon_b - \epsilon_c$ increased only weakly with increasing M. In the PPO–PS blends, the strain to produce crazing (ϵ_c) was found to be roughly constant for $0.5 < \phi < 0.68$ whereas the craze fibril stability increased markedly at values of $\phi \geq 0.64$. In all cases, the craze fibril breakdowns were traced to the formation of a small pear-shaped void at the craze/bulk interface. At the slow strain rates used in these experiments, craze breakdown is believed to occur by two events: (1) random chain scission to form the surfaces of the craze fibrils and (2) stress-mediated chain disentanglement of surviving strands *at the craze/bulk interface*. A revised microscopic statistical model, based on a detailed description of the craze microstructure, is found to be in satisfactory agreement with the empirically determined molecular weight (or ϕ) dependence of $\epsilon_b - \epsilon_c$.

Acknowledgment. The development of the revised statistical model of craze breakdown was done in collaboration with E. J. Kramer, and his important contributions are gratefully acknowledged. The author also acknowledges the careful experimental assistance of K. P. Leach and B. J. Wagner.

Appendix

Following ref 10, we now relate the P_{SD} in eq 10 to the microscopically determined Weibull parameters. We treat the strain ϵ at which craze fibril breakdown occurs, and consequently the strain at which an optically detectable void is observed, as a random variable with distribution function $P_b(\epsilon)$.[5,6] Accordingly, we suppose that the undeformed film square, with an initial volume V_o, contains randomly scattered flaws, which consist of intrinsic "weak spots" and to a far lesser extent foreign dust particles.

As a tensile strain ϵ is applied, crazes nucleate at $\epsilon = \epsilon_c$ and upon additional strain the craze/bulk peripheries expand. Concomitant with this growth is the formation of a "risk" volume of polymer V, which is defined as the fraction of V_o that has been transformed into craze fibrils at a plastic strain, ϵ_p ($=\epsilon - \epsilon_c$), i.e.

$$V = V_o\epsilon_p/(\lambda - 1) \tag{12}$$

where λ is the craze fibril extension ratio.[8-10]

The flaws that produce craze breakdown may be viewed as occurring as a compound Poisson process in space, the varying severity of the flaws giving rise to the compound feature. Now if the intrinsic weak spots are scattered at random throughout the film, the differential increase in V with infinitesimal increase in ϵ_p can be expressed as[5,6]

$$dV/d\epsilon_p = V_o/(\lambda - 1) \tag{13}$$

Next, we suppose that the craze drawing stress S increases roughly as a power law of the plastic strain, ϵ_p, viz.[5,6,10]

$$S = S_1\epsilon_p^{\delta} \tag{14}$$

where δ (>0) is a constant and S_1 is the value of S at $\epsilon_p = 1$. Moreover, since S is an increasing function of the plastic strain, ϵ_p, we assume the probability that a fibril breakdown occurs by chain scission and subsequent disentanglement within a given entanglement transfer length can be approximated by[10]

$$P_{SD}(\epsilon_p) \approx P_{SD}(S_1)\,\epsilon_p(\rho_w - 1) \tag{15}$$

Accordingly the mean number of intrinsic weak spots per unit volume can be expressed as

$$\Lambda(\epsilon_p) = n_f P_{SD}(\epsilon_p) \tag{16}$$

where n_f is the number of fibril elements formed from a unit risk volume V.

From arguments appropriate to a compound Poisson process,[35] one can show that the probability of forming

a void (via craze breakdown) at a strain ϵ_p may be given by[10]

$$p_b(\epsilon_p) = 1 - \exp\left[\int_0^{\epsilon_p} \epsilon^{(\rho_w - 1)} \frac{V_o n_f P_{SD}(S_1)}{\lambda - 1} d\epsilon \right] \quad (17)$$

where ρ_w ($=\delta + 1$) is the Weibull modulus. By integrating eq 17 and solving for $p_b = 0.5$, one can derive the following expression for the craze fibril stability ($\epsilon_b - \epsilon_c$), viz.

$$\epsilon_b - \epsilon_c = \left[\frac{(\lambda - 1)\rho_w \ln 2}{n_f V_o P_{SD}(S_1)} \right]^{1/\rho_w} \quad (18)$$

which is given as eq 10 in the text.

References and Notes

(1) Beahan, P.; Bevis, M.; Hull, D. *Polymer* **1973**, *14*, 1973.
(2) Murray, J.; Hull, D. *J. Polym. Sci., Part A-2* **1970**, *8*, 583.
(3) Kramer, E. J. *Polym. Eng. Sci.* **1984**, *24*, 761.
(4) Kramer, E. J. *Adv. Polym. Sci.* **1983**, *52/53*, 1.
(5) Yang, A. C.-M.; Kramer, E. J.; Kuo, C. C.; Phoenix, S. L. *Macromolecules* **1986**, *19*, 2010.
(6) Yang, A. C.-M.; Kramer, E. J.; Kuo, C. C.; Phoenix, S. L. *Macromolecules* **1986**, *19*, 2020.
(7) Henkee, C. S.; Kramer, E. J. *J. Polym. Sci., Part B: Polym. Phys.* **1984**, *22*, 721.
(8) Donald, A. M.; Kramer, E. J. *J. Polym. Sci., Part B: Polym. Phys.* **1982**, *20*, 899.
(9) Donald, A. M.; Kramer, E. J. *Polymer* **1982**, *23*, 461; **1982**, *23*, 1183.
(10) Kramer, E. J.; Berger, L. L. *Adv. Polym. Sci.* **1990**, *91/92*, 1.
(11) Berger, L. L.; Kramer, E. J. *Macromolecules* **1987**, *20*, 1980.
(12) Donald, A. M. *J. Mater. Sci.* **1985**, *20*, 2630.
(13) Plummer, C. J. G.; Donald, A. M. *J. Mater. Sci.* **1989**, *24*, 1399.
(14) Plummer, C. J. G.; Donald A. M. *J. Polym. Sci., Part B: Polym. Phys.* **1989**, *27*, 325.
(15) Berger, L. L. *Macromolecules* **1989**, *22*, 3162.
(16) Beahan, P.; Bevis, M.; Hull, D. *Proc. R. Soc. London A* **1975**, *343*, 525.
(17) Passaglia, E. *J. Phys. Chem. Solids* **1987**, *48* (No. 11), 1075.
(18) Doyle, M. J.; Maranci, A.; Orowan, E.; Stork, S. T. *Proc. R. Soc. London A* **1972**, *329*, 137.
(19) Schapery, R. A. *Int. J. Fract.* **1984**, *25*, 195; **1978**, *14*, 293; **1975**, *11*, 141.
(20) Kramer, E. J.; Hart, E. W. *Polymer* **1984**, *25*, 1667.
(21) Verheulpen-Heymans, N. *Polym. Eng. Sci.* **1984**, *24*, 809.
(22) Trassaert, P.; Schirrer, R. *J. Mater. Sci.* **1983**, *18*, 3004.
(23) Schirrer, R.; Le Masson, J.; Tomatis, B. *Polym. Eng. Sci.* **1984**, *24*, 820.
(24) Doll, W. *Adv. Polym. Sci.* **1983**, *52/53*, 105.
(25) Doyle, M. *J. Mater. Sci.* **1982**, *17*, 760; **1982**, *17*, 204.
(26) Koenczoel, L.; Hiltner, A.; Baer, E. *J. Appl. Phys.* **1986**, *60*, 2651.
(27) Berger, L. L.; Kramer, E. J. *J. Mater. Sci.* **1988**, *23*, 3536.
(28) Taylor, G. I. *Proc. R. Soc.* **1950**, *A210*, 192.
(29) Fields, R. J.; Ashby, M. F. *Philos. Mag.* **1976**, *33*, 33.
(30) Argon, A. S.; Salama, M. M. *Philos. Mag.* **1977**, *36*, 1217.
(31) Kuo, C. C.; Phoenix, S. L.; Kramer, E. J. *J. Mater. Sci. Lett.* **1985**, *4*, 459.
(32) These estimates of M_n', within the crazed material, are on the order of that recently measured using GPC; see: Willett, J. L.; O'Connor, K. M.; Wool, R. P. *J. Polym. Sci., Part B: Polym. Phys.* **1986**, *24*, 2583.
(33) The form of t_{dis} given in eq 7, derived by Kramer and Berger,[10] is consistent with a forced reptation model of chain disentanglement at the craze/bulk interface. The predicted scaling of this equation differs from that first proposed by McLeish et al.,[34] who apparently failed to consider the increase in M_e with chain disentanglement.
(34) McLeish, T. C. B.; Plummer, C. J. G.; Donald, A. M. *Polymer* **1989**, *30*, 1651.
(35) Karlin, S.; Taylor H. M. *A Second Course in Stochastic Processes*, 1st ed.; Academic: New York, 1982; pp 426–441.
(36) Consistent with eq 3, the number-average molecular weight of the chains in the fibril in which i strands remain unbroken can be computed from $M(i) = [1/M_n + (1 - (iq/n_e))/M_e]^{-1}$.
(37) Over the composition range $0.5 \leq \phi \leq 0.68$ and at a constant $T_g - T$, the monomeric friction coefficient of PPO is assumed to be only weakly dependent on ϕ.
(38) The proposed model also offers a convenient and logical framework for quantitatively describing the marked deleterious effects of (rigid) foreign particulate. For example, if a given sample contains stress concentrating particles that affect a volume fraction Φ of the film, then the revised (volume-averaged) P_{SD} in eq 10 can be expressed as

$$P_{SD}(S_1) = (1 - \Phi)P_{SDF}(S_1) + \Phi P_{SDC}(S_1)$$

where $P_{SDF}(S_1)$ is the fibril failure probability of the unaffected film and $P_{SDC}(S_1)$ is the fibril failure probability in the region affected by the stress concentration around the dust particle. Since only a small stress concentration can increase the $P_{SD}(S_1)$ by several orders of magnitude, a small volume fraction of particulate can have pronounced effects. (See ref 10.)
(39) Composto, R. J.; Kramer, E. J.; White, D. M. *Bull. Am. Phys. Soc.* **1987**, *32* (No. 3), 663.
(40) Graessley, W. W. *Adv. Polym. Sci.* **1974**, *16*, 55.
(41) Miller, P.; Kramer, E. J. Deformation, Yield and Fracture of Polymers. *Proceedings of the Plastics rubber Institute Conference* Churchill College: Cambridge, U.K., 1988; Vol. 81/1.
(42) Miller, P. Ph.D. Thesis, Cornell University, Ithaca, NY, 1987.

Registry No. PMMA, 9011-14-7; PαMS, 25014-31-7; PS, 9003-53-6; PPO (SRU), 24938-67-8; PPO (homopolymer), 25134-01-4.